Grain refinement of cast peritectic TiAl-based alloy by solid-state phase transformations

K. Kamyshnykova[1,2]*, J. Lapin[1]

[1]*Institute of Materials and Machine Mechanics, Slovak Academy of Sciences, Dúbravská cesta 9, 845 13 Bratislava, Slovak Republic*
[2]*Slovak University of Technology in Bratislava, Paulínska 16, 917 24 Trnava, Slovak Republic*

Abstract

The effect of solid-state phase transformations on grain refinement of cast peritectic TiAl-based alloy with nominal composition Ti-47Al-5Nb-0.2B-0.2C (at.%) has been investigated. Three multi-stage heat treatment routes consisting of pretreatment in single α phase field followed by air, oil or water cooling and subsequent annealing in $\alpha + \gamma$ or single α fields were applied to refine grain structure of the alloy. The microstructure of the as-cast samples consists of coarse fully lamellar $\alpha_2(Ti_3Al) + \gamma(TiAl)$ grains with a grain size of 1310 μm. The annealing of the pretreated samples consisting of massive γ_M and fine lamellar $\alpha_2 + \gamma$ grains in the $\alpha + \gamma$ phase field leads to the formation of a duplex type of microstructure composed of lamellar $\alpha_2 + \gamma$ and single γ phase grains with a grain size ranging from 14 to 22 μm. The solution annealing in the single α phase field of the pretreated samples aged in the $\alpha + \gamma$ phase field leads to the formation of fully lamellar $\alpha_2 + \gamma$ grains with a grain size ranging from 395 to 472 μm.

1. Introduction

Intermetallic TiAl-based alloys are promising structural materials for high-temperature aerospace and automotive industry applications up to about 750 ℃ [1–6]. Depending on their chemical composition and processing parameters, these alloys can be produced with four different types of microstructure: near-gamma (NG), duplex (DP), near lamellar (NL) and fully lamellar (FL). The DP/NG alloys are characterised by higher room temperature (RT) tensile strength, ductility and longer fatigue life than FL/NL ones [7]. On the other hand, the FL/NL alloys exhibit better creep resistance, higher fracture toughness and crack propagation resistance than DP/NG structures [8, 9]. However, a coarse-grained lamellar structure results in low RT tensile strength and ductility [7, 10]. The yield strength and ductility of TiAl-based alloys can be significantly increased by decreasing grain size [11]. On the other hand, Parthasarathy et al. [12] and

Maruyama et al. [13] have reported that the grain size ranging from 70 to 1200 μm has negligible or no effect on creep behaviour of FL alloys. Kim and Kim [14] have shown that a good balance between RT mechanical properties and high temperature creep resistance can be achieved by an appropriate heat treatment leading to a fully lamellar equiaxed grain structure with a grain size of about 280 μm.

Basically, two main approaches have been investigated to refine the coarse-grained structure of as-cast TiAl-based alloys: (i) solid-state phase transformations and (ii) alloying with minor additions. Numerous research works have been published on grain refinement based on solid-state phase transformations and particularly on non-equilibrium phase transformations [15–23]. Indeed, a large range of microstructures can be obtained by varying the cooling rate from the α (Ti-based solid solution with A3 crystal structure) phase field ranging from the equilibrium lamellar structure to the Widmanstätten structure, feath-

Ta b l e 1. The chemical composition of as-cast samples (at.%)

Ti	Al	Nb	B	C	O	H	N
47.6 ± 0.3	46.5 ± 0.4	5.3 ± 0.2	0.22 ± 0.02	0.22 ± 0.02	0.14 ± 0.02	0.010 ± 0.003	0.010 ± 0.003

ery structure, massive structure and finally the highly metastable retained α structure. The massive structure has been used as a precursor for subsequent heat treatments because it leads to a refined and isotropic structure [24–26]. The massive transformation is the diffusionless transformation of the α phase to massive γ_M (TiAl) which strongly depends on Al content and is significantly influenced also by alloying additions. The alloying elements showing low diffusivity in both TiAl and Ti$_3$Al phases decrease critical cooling rates required for the formation of massive γ_M [19]. Some TiAl-based alloys have been specifically designed, as the "air hardenable" requiring only air cooling from the single α phase field to be fully transformed to massive γ_M [10, 27–31]. However, many TiAl-based alloys do not exhibit massive transformation or this transformation is shifted to very high cooling rates. Therefore, alternative heat treatment processes based on solid-state phase transformations of the retained α have been developed to refine the coarse-grained structure and optimise their mechanical properties [32].

Hu et al. [33, 34] have reported that low boron additions are very effective to refine the grain structure of TiAl-based alloys. Recently Kamyshnykova and Lapin [35] have shown that low addition of boron was ineffective to refine coarse-grained structure hypoperitectic and peritectic TiAl-based alloys prepared by vacuum induction melting in graphite crucibles and casting into graphite moulds. Since the coarse lamellar grain structure reduces RT ductility and tensile strength significantly, additional processing routes based on solid-state phase transformations need to be developed to refine the grain structure of such peritectic type of TiAl-based alloys.

This study aims to evaluate the effect of solid-state phase transformations on grain refinement of cast peritectic TiAl-based alloy with a nominal composition Ti-47Al-5Nb-0.2B-0.2C (at.%). In this alloy, niobium is added to improve oxidation resistance, creep strength and tensile strength [36]. Minor additions of boron and carbon were added to influence grain structure formation and improve creep resistance, respectively [37–39].

2. Experimental procedure

Table 1 shows the measured chemical composition of the studied alloy. The as-cast bar was machined to smaller samples with a diameter of 17 mm and length of 26 mm using wire electrical discharge machining.
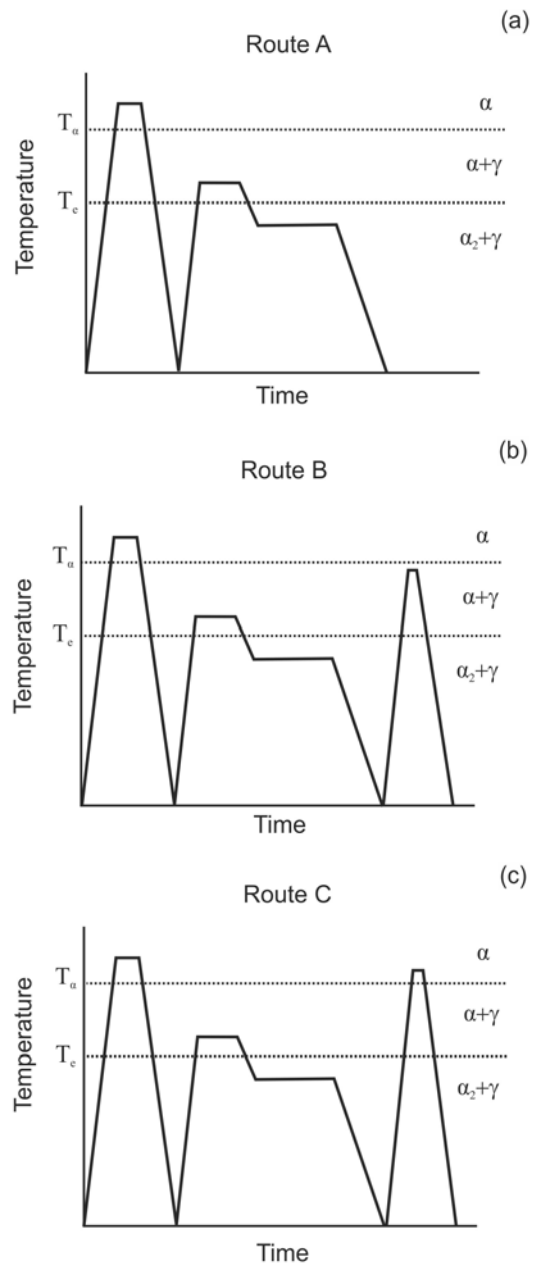

Fig. 1. Schematic views of heat treatment routes applied in the present study: (a) heat treatment route A; (b) heat treatment route B; (c) heat treatment route C. T_α is α phase transition temperature; T_e is eutectoid temperature.

The samples were heated to a solution annealing temperature of 1405 °C at a heating rate of 10 °C min^{-1}, held at this temperature for 1 h and cooled to room temperature using forced air cooling, oil quenching
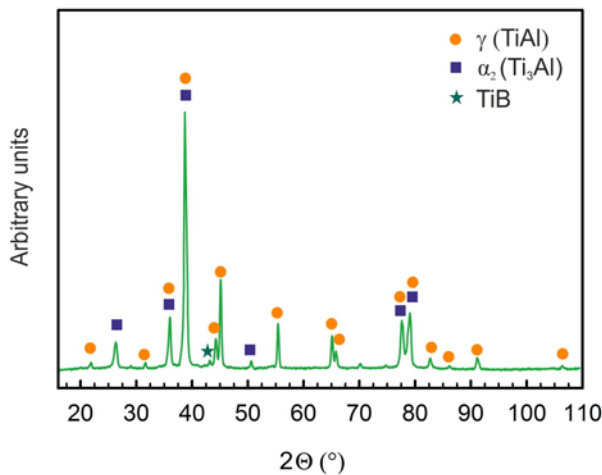
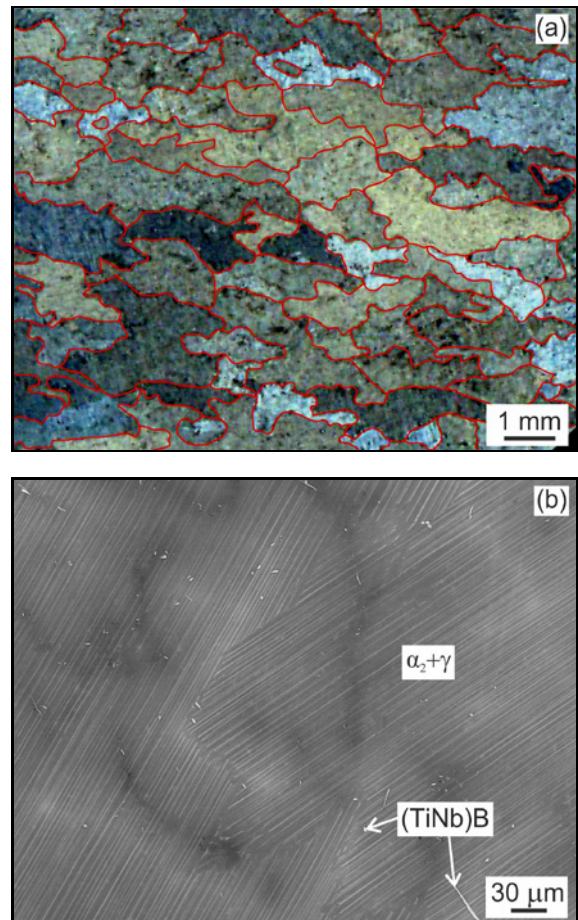Fig. 2. The typical XRD pattern of the as-cast samples.

Fig. 3. Macrostructure and microstructure of the as-cast samples: (a) coarse equiaxed and elongated grains, LM; (b) a fully lamellar microstructure with numerous borides, BSE.

and water quenching which resulted in average cooling rates of 15, 24 and 48 °C s^{-1}, respectively [31]. The air cooled (AC), oil quenched (OQ) and water quenched (WQ) samples were subjected to three different heat treatment routes designated as A, B, and C, as seen in Fig. 1. The heat treatment route A consisted of the heating of the pretreated AC, OQ and WQ samples to an annealing temperature of 1225 °C at a heating rate of 10 °C min^{-1}, holding in $\alpha + \gamma$ phase field at 1225 °C for 4 h, cooling to a temperature of 900 °C at a cooling rate of 10 °C min^{-1}, holding in $\alpha_2 + \gamma$ phase field at 900 °C for 20 h and furnace cooling to room temperature, as shown in Fig. 1a. The heat treatment route B included the route A which was followed by the heating of the samples to a temperature of 1360 °C at a heating rate of 10 °C min^{-1}, holding in $\alpha + \gamma$ phase field at 1360 °C for 0.5 h, cooling to a temperature of 700 °C at a cooling rate of 10 °C and furnace cooling to room temperature, as shown in Fig. 1b. The heat treatment route C included the route A which was followed by the heating of the samples to a temperature of 1385 °C at a heating rate of 10 °C min^{-1}, holding in single α phase field at 1385 °C for 0.5 h, cooling to a temperature of 700 °C at a cooling rate of 10 °C min^{-1} and furnace cooling to room temperature, as shown in Fig. 1c.

The heat treatments were carried out in a resistance furnace under an argon atmosphere. The temperature of the samples was measured by PtRh10-Pt thermocouple touching the specimen surface.

Metallographic preparation of the samples consisted of conventional grinding using abrasive papers, polishing on diamond pastes with various grain size up to 1 μm and etching in a solution of 100 ml H$_2$O, 6 ml HNO$_3$ and 3 ml HF. Microstructure evaluation was performed by light microscopy (LM), scanning electron microscopy (SEM) and scanning electron microscopy in back-scattered electron (BSE) mode. Oxy-

gen, hydrogen and nitrogen contents were measured by LECO ONH836, and carbon content was determined by LECO CS844 elemental analysers. The chemical composition of the samples was evaluated by energy-dispersive spectroscopy (EDS). The X-ray diffraction (XRD) analysis of coexisting phases was carried out by a diffractometer Bruker D8 equipped with X-ray tube with rotating Cu anode operating at 12 kW. Volume fraction of phases was measured by computerised image analysis using digitalised micrographs. The grain size was measured by a linear intercept method, and the measured data were treated statistically.

3. Results and discussion

3.1. Microstructure and grain size of as-cast samples

Figure 2 shows the typical XRD pattern of the Ti-46.5Al-5.3Nb-0.22B-0.22C (at.%) samples indicating the presence of three consisting phases: γ(TiAl),
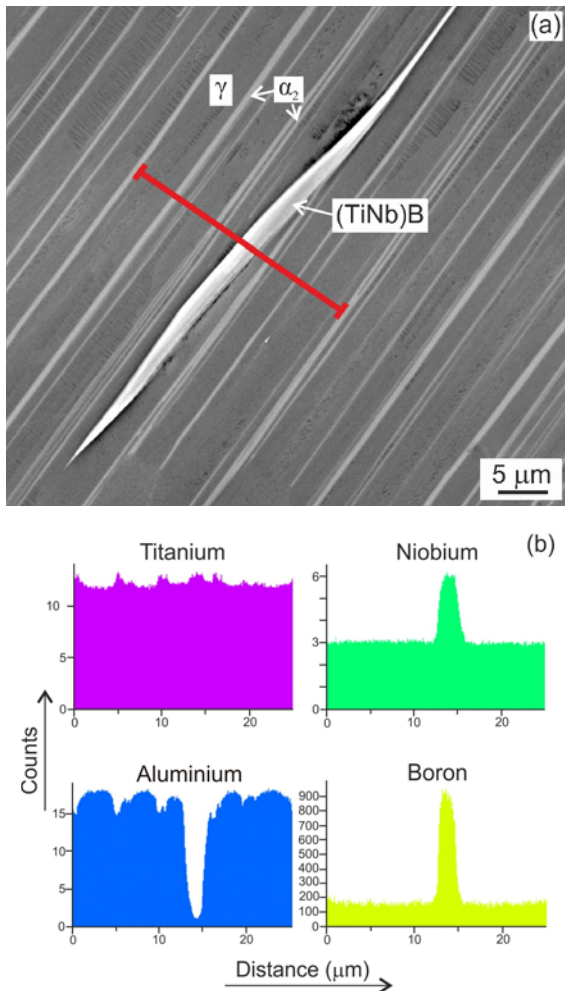
Fig. 4. (a) BSE micrograph showing the position of the line EDS analysis through the boride particle and well-aligned α_2 and γ lamellae; (b) distribution of titanium, aluminium, niobium and boron along the analysed line shown in Fig. 3a.

Fig. 5. The log-normal distribution function of initial grain size of the as-cast samples.

α_2(Ti$_3$Al) and TiB. The macrostructure and microstructure of the as-cast samples are shown in Fig. 3. The coarse equiaxed and elongated grains consist of well-aligned lamellae and numerous boride particles, as seen in Figs. 3a,b. Figure 4 shows the detail of the lamellar $\alpha_2 + \gamma$ microstructure with the position of the line EDS analysis. The line EDS analysis indicates positions of the γ lamellae characterised by an increased aluminium content, α_2 lamellae by an increased content of titanium and boride particle by an increased content of boron and niobium, as shown in Figs. 4a,b. The average chemical composition of the boride particles measured by EDS is Ti-10Nb-56B (at.%) and corresponds to Ti:Nb ratio of 3.4:1. Therefore, the most appropriate formula for the boride particle can be expressed as (Ti,Nb)B that reflects the complex monoboride compound formation during solidification. However, the measured composition of the

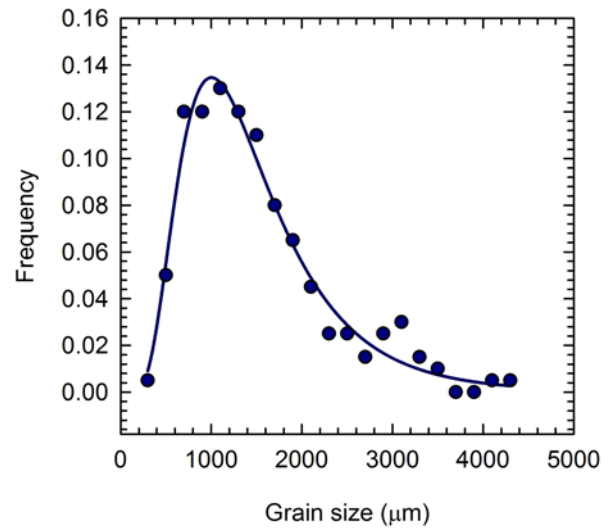boride particles is only indicative due to the fundamental restriction regarding the low sensitivity of the EDS analysis to the determination of light elements including boron. Cheng [40] has reported that the Ti:Nb ratio in the boride particles alloys corresponds to 3:1 in Ti-8Nb-xB (at.%) alloys. Kartavykh et al. [41] have reported different Ti:Nb ratio corresponding to 1:1 in the boride particles formed in directionally solidified Ti-44Al-7Nb-2B (at.%) alloy measured by calibrated Auger spectroscopy. Figures 3a and 3b clearly indicate that the alloying with boron is ineffective to refine the coarse-grained structure of the studied alloy. Hecht et al. [37] have reported that the grain refinement with low boron additions fails when the peritectic reaction is a part of the solidification path because the peritectic α grains formed during growth from the liquid invade the microstructure through the subsequent solid-state transformations. The statistical analysis of the measured grain size (about 500 measurements) can be fitted by a log-normal distribution function characterised by a median value of (1310 ± 30) µm, as shown in Fig. 5. The correlation coefficient of this fit is $r^2 = 0.97$. Such large grain size leads to a very low RT tensile strength and ductility of the studied alloy and needs to be refined by appropriate heat treatments.

3.2. Effect of continuous cooling from α phase field on the microstructure

Figure 6 shows the microstructure of the samples after the pretreatment consisting of solution annealing in the single α phase field at 1405 °C for 1 h followed by the air cooling, oil quenching and water quenching. The cooling rate of 15 °C min^{-1} in the AC sample
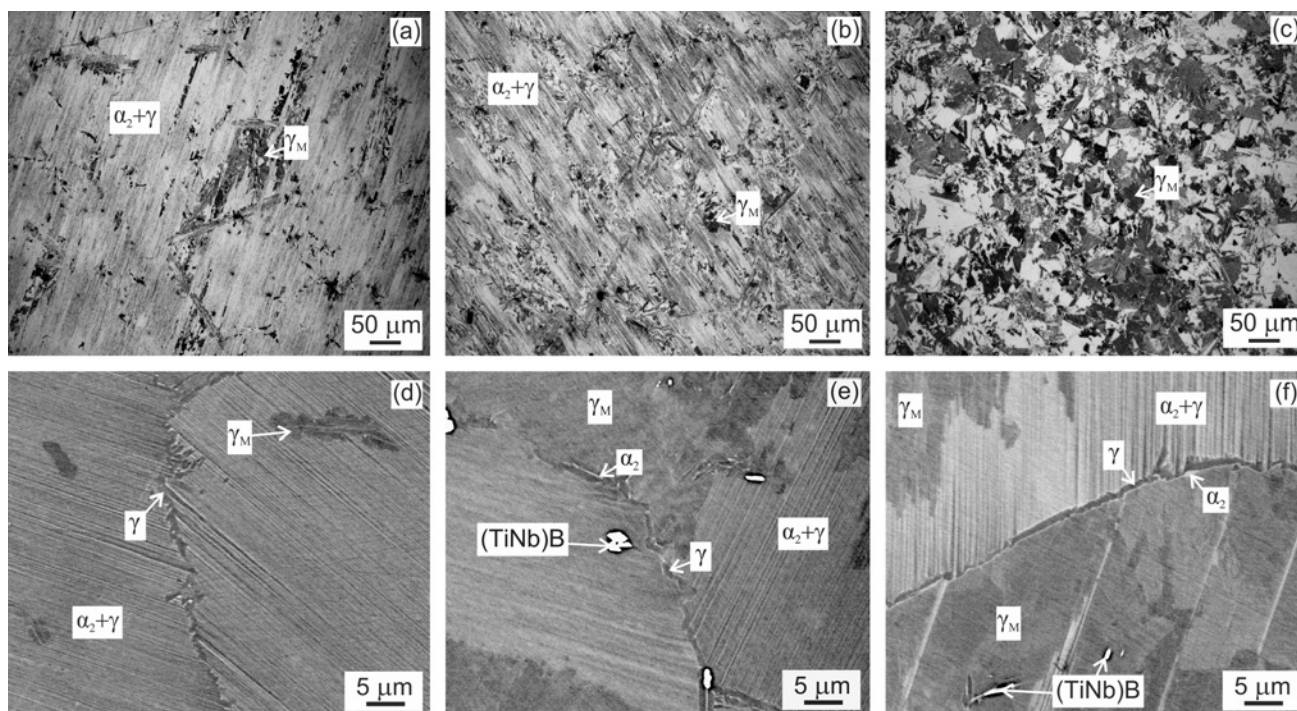
Fig. 6. Microstructures after cooling from solution annealing temperature of 1405 °C using air cooling, oil quenching and water quenching: (a) AC sample, LM; (b) OQ sample, LM; (c) WQ sample, LM; (d) BSE micrograph showing grain boundary of AC sample; (e) BSE micrograph showing grain boundary of OQ sample; (f) BSE micrograph showing grain boundary of WQ sample.

results in the transformation of the α phase to fine lamellar $\alpha_2 + \gamma$ microstructure with the low volume fraction of the massive γ_M (7 vol. %) forming predominantly intragranularly, as illustrated in Figs. 6a,d. The higher cooling rate of $24\,°C\,s^{-1}$ in the OQ sample leads to the formation of lamellar $\alpha_2 + \gamma$ microstructure with a higher volume fraction of the massive γ_M (33 vol.%) compared to that of the AC sample, as seen in Fig. 6b. Although the massive γ_M is still nucleated preferentially intragranularly, its nucleation activity at the grain boundaries increases, as seen in Fig. 6e. Further increase of the cooling rate to $48\,°C\,s^{-1}$ in the WQ sample leads to an increase of volume fraction of the massive γ_M to 48 vol.% and transformation of the remaining α phase to fine lamellar microstructure, as seen in Figs. 6c and 6f. In this case, the massive γ_M is formed intragranularly as well as along some grain boundaries (Fig. 6f).

The main controlling factors affecting the massive transformation in TiAl-based alloys are initial microstructure, chemical composition, cooling rate, solution annealing temperature and time. Although intragranular nucleation of massive γ_M has been reported during continuous cooling from α phase field [26], it is generally accepted that the nucleation occurs predominantly at α/α grain boundaries [42, 43]. The γ_M nuclei generally exhibit a Blackburn orientation relationship with one of the adjacent α grains while they

grow at the expense of the other grain by the movement of highly mobile incoherent interfaces. The γ_M domains contain a high density of lattice defects such as dislocations, stacking faults, fine twins, and antiphase boundaries. The present study indicates that the intragranular nucleation of the massive γ_M occurs preferentially in the AC and OQ samples. The majority of the grain boundaries contain single γ phase which clearly reduces the nucleation activity of the massive γ_M, as shown in Figs. 6d,e. The nucleation of the massive γ_M at the grain boundaries is more frequent in the WQ samples. In this case, the grain boundary γ is still preserved but it is separated by a thin layer of the α phase at which the γ_M nucleates and then propagates within the grain. However, the adjacent α grain transforms to fine fully lamellar $\alpha_2 + \gamma$ microstructure, as seen in Fig. 6f. The formation of the grain boundary γ has also been reported by Huang et al. [17] in Ti-46Al-8Nb (at.%) alloy cooled from the α phase field at a nominal cooling rate of $40\,°C\,s^{-1}$. The formation of lamellar microstructure in the WQ sample indicates that the cooling rate of $48\,°C\,s^{-1}$ is still too low to suppress diffusion assisted transformation of the α phase to the lamellar structure and to promote formation of higher volume fraction of the massive γ_M or to preserve untransformed α phase in the microstructure similarly to that observed by several authors [28, 31].
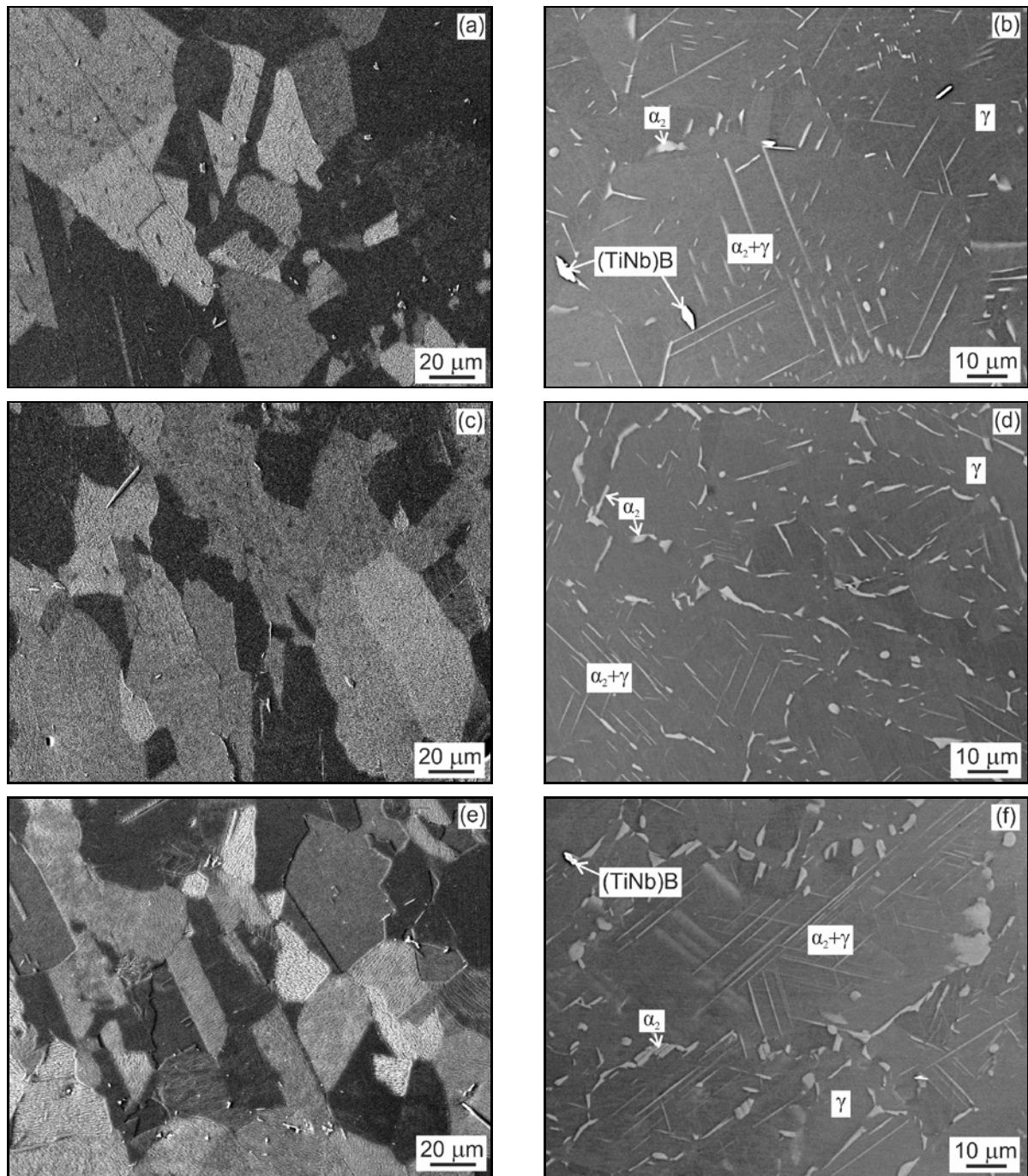
Fig. 7. Microstructure of the AC, OQ and WQ samples after the heat treatment route A: (a) grain structure of the AC sample, SEM; (b) convoluted microstructure of the AC sample, BSE; (c) grain structure of the OQ sample, SEM; (d) convoluted microstructure of the OQ sample, BSE; (e) grain structure of the OQ sample, SEM; (f) convoluted microstructure of the WQ sample, BSE.

3.3. Effect of heat treatment routes on microstructure and grain size

3.3.1. Heat treatment route A

Figure 7 shows the microstructure of the AC, OQ and WQ samples subjected to the heat treatment route A. The annealing temperature of 1225 °C cor-

responds to the $\alpha + \gamma$ phase field of the studied alloy and leads to the formation of a high volume fraction of the γ phase. The stabilisation annealing in $\alpha_2 + \gamma$ phase field at 900 °C leads to the growth of secondary α_2 lamellae in the γ matrix. After the annealing, the microstructure of the samples consists of refined grains with well-defined grain boundaries, as shown in Figs. 7a,c,e. Two types of microstructures can be
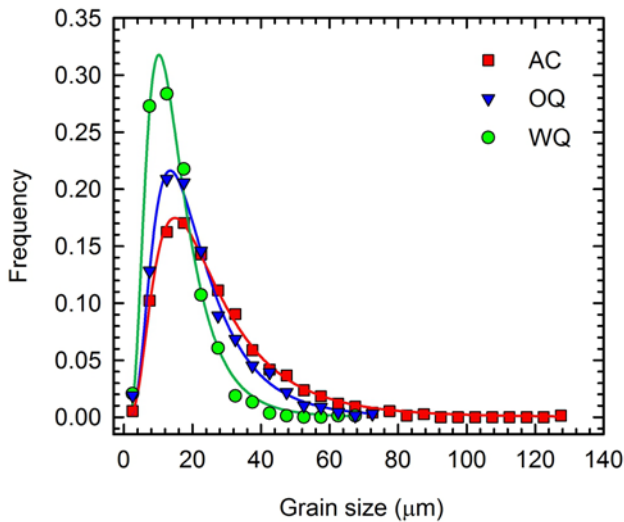
Fig. 8. Log-normal grain size distribution of the AC, OQ and WQ samples after the heat treatment route A.

Fig. 9. Dependence of grain size of the AC, OQ and WQ samples on the applied heat treatment routes A, B and C.

identified within the refined grains such as single γ phase and two-phase $\alpha_2 + \gamma$, as shown in Figs. 7b,d,f. The $\alpha_2 + \gamma$ grains contain either low volume fraction of partially dissolved aligned or fine crossed α_2 lamellae. The grain boundaries of both types of grains are covered by coarsened α_2 phase. The statistical analysis of the measured grain size of the AC, OQ and WQ samples (about 800 measurements for each sample) leads to log-normal distribution functions, as shown in Fig. 8. The correlation coefficients of these fits are better than $r^2 = 0.98$. The distribution curves indicate that a higher volume fraction of the massive γ_M leads to a more homogeneous distribution of the grain size in the annealed samples. While the grains with a size of about 120 μm are preserved in the microstructure of the AC samples, the maximum measured grain size is only about 70 μm in the WQ sample. Figure 9 shows the dependence of median grain size on the applied heat treatment route. The decrease of the grain size from 22.4 to 13.7 μm in the samples subjected to the heat treatment route A can be related to an increase of the volume fraction of the massive γ_M from 7 to 48 vol.%.

Two main mechanisms are responsible for the grain refinement during annealing at 1225 °C. The first mechanism is the formation of the refined grains with the convoluted type of microstructure during the transformation of the unstable massive γ_M by the precipitation of the α plates with four crystallographic variants on {111} crystallographic planes of the γ phase with tetragonal crystal structure L1$_0$, as shown in Fig. 7f [28]. The second mechanism responsible for the grain refinement is the discontinuous coarsening leading to the formation of lamellar grains with coarse lamellar microstructure and single γ phase grains due
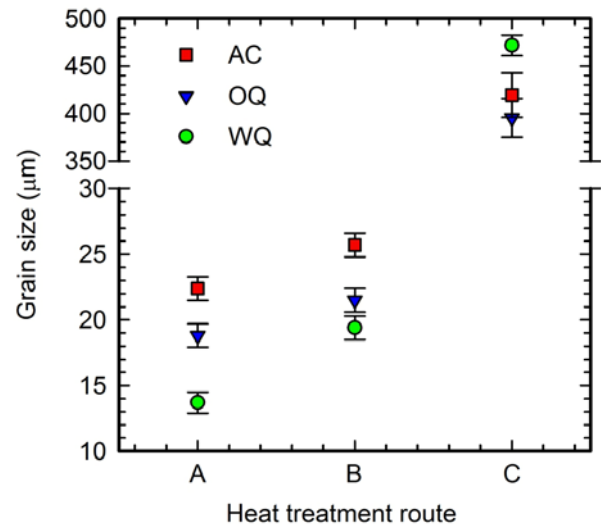
to highly stable interfaces of the primary fine lamellar microstructure [44, 45]. The discontinuous reaction occurs at the grain boundaries and within the original fine lamellar colonies of the AC, OQ and WQ samples. The driving force for the discontinuous coarsening is a reduction of α/γ interface energy by increasing interlamellar spacing, change of chemical composition and volume fraction of coexisting phases to attain phase equilibrium [44].

3.3.2. Heat treatment route B

Figure 10 shows microstructure of the AC, OQ and WQ samples subjected to the heat treatment route B. The selected annealing temperature of 1360 °C corresponds to the $\alpha + \gamma$ phase field of the studied alloy and leads to the formation of a high volume fraction of the α phase. The duplex type of microstructure of the AC, OQ and WQ samples consists of refined grains with two types of a microstructure such as single γ phase and lamellar $\alpha_2 + \gamma$, as shown in Figs. 10a–c. The grain boundaries contain coarsened α_2 particles. The duplex type of microstructure formed during the heat treatment route B is very similar to that of Ti-47Al-2Nb-2Cr (at.%) alloy reported recently by Thomas and Bacos [46]. The statistical analysis of the measured grain size of the AC, OQ and WQ samples (about 800 measurements for each sample) leads to log-normal distribution functions, as shown in Fig. 11. The correlation coefficients of these fit are better than $r^2 = 0.98$. The distribution curves indicate that the volume fraction of the massive γ_M has no significant effect on the distribution of the measured grain size after the heat treatment route B. The median grain size ranging from 16.0 to 18.4 μm indicates that this
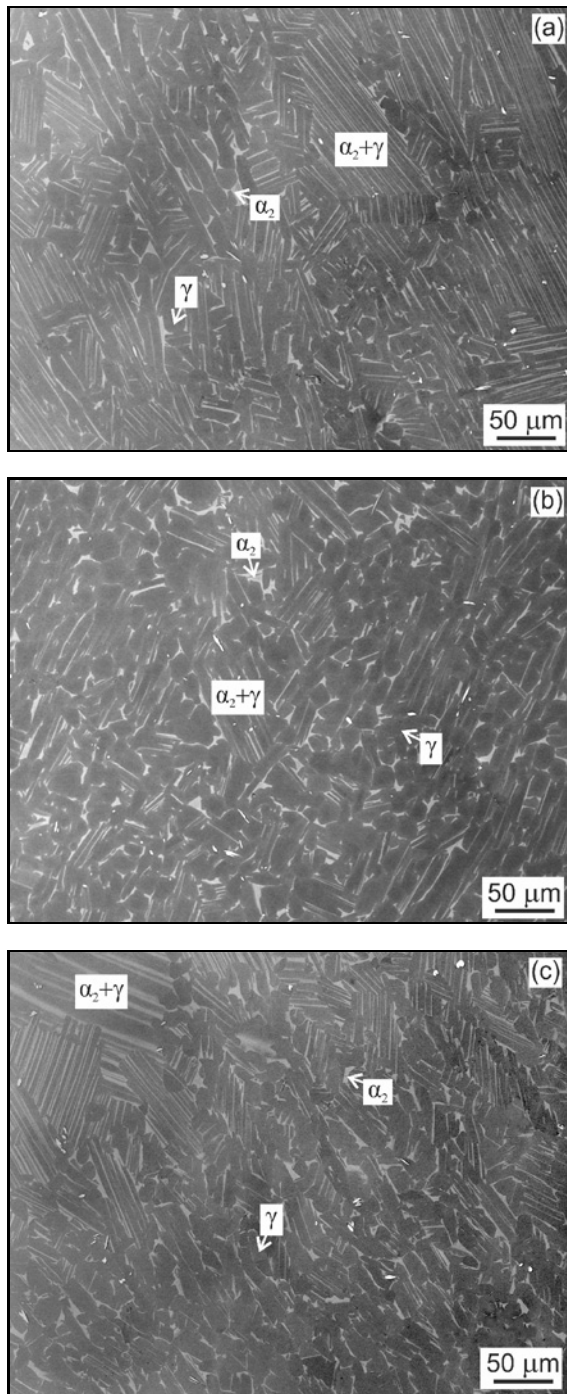
Fig. 10. BSE micrographs showing duplex microstructure after the heat treatment route B: (a) AC sample; (b) OQ sample; (c) WQ sample.

Fig. 11. Log-normal grain size distribution of the AC, OQ and WQ samples after the heat treatment route.

additional annealing step in the $\alpha + \gamma$ phase field at 1360 °C has a negligible effect on the grain size compared to that of the samples subjected to the heat treatment route A.

3.3.3. Heat treatment route C

Figure 12 shows the microstructure of the AC,
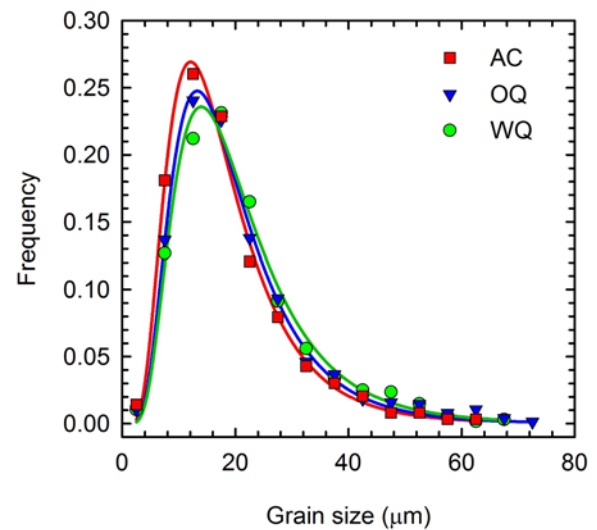
OQ and WQ samples subjected to the heat treatment route C. The selected annealing temperature of 1385 °C corresponds to the single α phase field of the studied alloy. The microstructure of the samples consists of coarse lamellar $\alpha_2 + \gamma$ grains, as shown in Figs. 12a–c. Formation of the fully lamellar microstructure results from the precipitation of γ lamellae in either the disordered α or ordered α_2 matrix [47]. During the continuous cooling from the single α phase field the formation of the γ lamellae starts in the $\alpha + \gamma$ phase field and is finalised in the $\alpha_2 + \gamma$ phase field. The whole sequence of the lamellar structure formation involves change of the crystal structure from hcp to fcc by propagation of Shockley partial dislocations in the α matrix, chemical composition change by atom transfer by a combined shear and diffusion process and ordering reaction of fcc structure leading to the final tetragonal L1$_0$ structure of the γ phase [47]. The statistical analysis of the measured grain size of the AC, OQ and WQ samples leads to log-normal distribution functions, as seen in Fig. 13. The correlation coefficients of these fits are better than $r^2 = 0.97$. The distribution curves indicate that the grain growth is faster in the WQ sample exhibiting a narrow grain size distribution after the heat treatment route A. The median grain size of 472 µm measured in the WQ sample is higher than those of 419 and 395 µm of the AC and OQ samples, respectively. The main mechanism affecting the grain structure of the AC, OQ and WQ samples during annealing in the α phase field is the growth of the α grains which can be described by an equation in the form [48]:
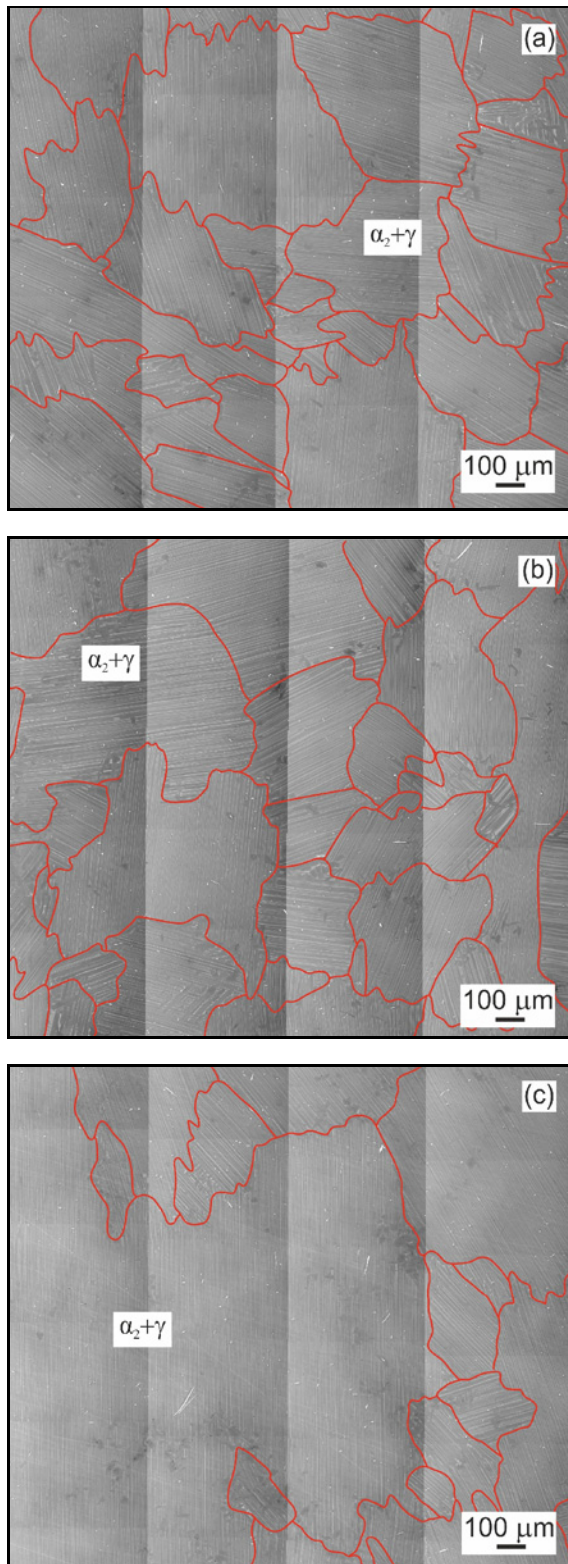
$$d = kt^n \exp\left(-\frac{Q}{RT}\right), \qquad (1)$$

Fig. 12. BSE micrographs showing fully lamellar microstructure after the heat treatment route C: (a) AC sample; (b) OQ sample; (c) WQ sample.
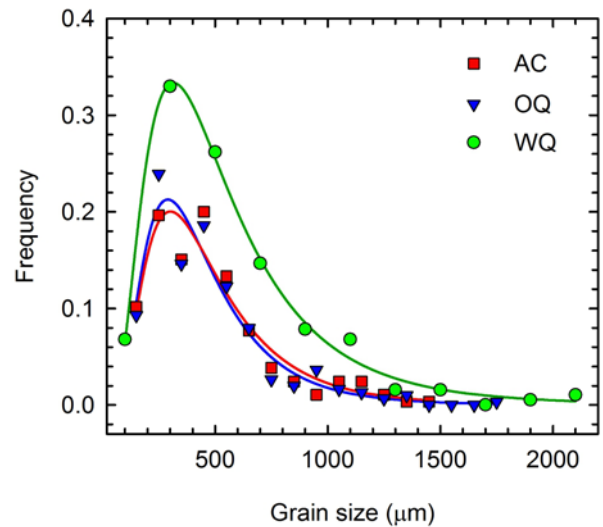

Fig. 13. Log-normal grain size distribution of the AC, OQ and WQ samples after the heat treatment route C.

is the activation for grain growth, R is the universal gas constant, and T is the absolute temperature. As shown by Lapin and Klimová [48, 49] and Zhang et al. [50], the annealing in the α phase field leads to a fast growth of α grains which growth kinetics is characterised by the activation energy for grain growth of $Q = 145\,\mathrm{kJ\,mol^{-1}}$ and time exponent of $n = 0.36$. Since the annealing temperature of 1385 °C is selected to be very close to $\alpha \rightarrow \alpha + \gamma$ transition temperature, the annealing time needs to be shortened to prevent undesirable grain growth and preserve smaller fully lamellar grains in the studied alloy. A grain size up to about 280 μm has been suggested by Kim and Kim [14, 51] to maintain an optimal balance between the room and high-temperature mechanical properties of TiAl-based alloys.

It should be noted that the fast cooling rates occasionally lead to the formation of short cracks in the OQ and even long cracks in WQ samples [31]. Hence, such type of cooling could not be applied for the grain refinement of cast components in practice. Hence, air cooling leading to the formation of the only low volume fraction of the massive γ_M and fine lamellar microstructure combined with additional annealing in the $\alpha + \gamma$ or α phase fields can be considered to be a perspective method for the grain refinement of the studied peritectic alloy [52].

4. Conclusions

The effect of solid-state phase transformations on grain refinement of cast peritectic TiAl-based alloy has been studied. The following conclusions are reached:
1. The initial microstructure of as-cast samples

where d is the grain size, k is the material constant, t is the annealing time, n is the time exponent, Q

consists of coarse fully lamellar $\alpha_2 + \gamma$ grains characterised by a median grain size of 1310 µm. The boride (Ti,Nb)B particles are found to be ineffective to refine the microstructure of the alloy during solidification and solid-state phase transformations.

2. The pretreatment of the samples consisting of solution annealing in the α phase field followed by fast cooling leads to the formation of massive γ_M and fine lamellar microstructure. The volume fraction of the massive γ_M depends on the cooling medium and increases from 7 to 48 vol.% by increasing the cooling rate from 15 to $48\,°C\,s^{-1}$.

3. The heat treatment route A composed of the pretreatment and subsequent annealing of the samples in the $\alpha+\gamma$ phase field leads to the formation of refined grain structure consisting of single γ and convoluted $\alpha_2 + \gamma$ grains characterised by a grain size ranging from 14 to 22 µm. The grain boundaries are found to be covered by coarsened α_2 phase.

4. The heat treatment route B composed of the heat treatment route A and subsequent annealing in the $\alpha+\gamma$ phase field leads to the formation of a refined duplex type of microstructure consisting of single γ and lamellar $\alpha_2 + \gamma$ grains characterised by a grain size ranging from 16 to 18 µm. The grain boundaries are found to be covered by coarsened α_2 phase.

5. The heat treatment route C composed of the heat treatment route A and subsequent annealing in the single α phase field leads to the formation of coarse grains with fully lamellar $\alpha_2 + \gamma$ microstructure and grain size ranging from 395 to 472 µm.

Acknowledgements

References

[1] Haun, R. E.: JOM, *69*, 2017, p. 2615. doi:10.1007/s11837-017-2578-1

[2] Bewlay, B. P., Nag, S., Suzuki, A., Weimer, M. J.: Mater. High Temp., *33*, 2016, p. 549. doi:10.1080/09603409.2016.1183068

[3] Tetsui, T., Ono, S.: Intermetallics, *7*, 1999, p. 689. doi:10.1016/S0966-9795(98)00085-5

[4] Wu, X.: Intermetallics, *14*, 2006, p. 1114. doi:10.1016/j.intermet.2005.10.019

[5] Bünck, M., Stoyanov, T., Schievenbusch, J., Michels, H., Gußfeld, A.: JOM, *69*, 2017, p. 2565. doi:10.1007/s11837-017-2534-0

[6] Liang, Y., Lin, J.: JOM, *69*, 2017, p. 2571. doi:10.1007/s11837-017-2551-z

[7] Kim, Y.-W.: Intermetallics, *6*, 1998, p. 623. doi:10.1016/S0966-9795(98)00037-5

[8] Appel, F., Wagner, R.: Mater. Sci. Eng. R, *22*, 1998, p. 187. doi:10.1016/S0927-796X(97)00018-1

[9] Dimiduk, D. M., Martin, P. L., Kim, Y. W.: Mater. Sci. Eng. A, *243*, 1998, p. 66. doi:10.1016/S0921-5093(97)00780-6

[10] Lapin, J., Gabalcova, Z., Bajana, O., Pelachova, T., Stanekova, H., Frkanova, K.: In: Proceedings of the Gamma Titan. Alum. Alloy. Eds.: Kim, Y.-W., Wilfried, S., Lin, J., Dimiduk, D., Appel, F.: TMS (The Minerals, Metals & Materials Society), 2014, p. 179. doi:10.1002/9781118998489.ch25

[11] Dimiduk, D. M., Hazzledine, P. M., Parthasarathy, T. A., Seshagiri, S., Mendiratta, M. G.: Metall. Mater. Trans. A Phys. Metall. Mater. Sci., *29*, 1998, p. 37. doi:10.1007/s11661-998-0157-3

[12] Parthasarathy, T., Mendiratta, M., Dimiduk, D. M.: Scr. Mater., *37*, 1997, p. 315. doi:10.1016/S1359-6462(97)00099-7

[13] Maruyama, K., Yamamoto, R., Nakakuki, H., Fujitsuna, N.: Mater. Sci. Eng. A, *239–240*, 1997, p. 419. doi:10.1016/S0921-5093(97)00612-6

[14] Kim, Y. W., Kim, S. L.: Intermetallics, *53*, 2014, p. 92. doi:10.1016/j.intermet.2014.04.006

[15] Srivastava, D., Hu, D., Chang, I. T. H., Loretto, M. H.: Intermetallics, *7*, 1999, p. 1107. doi:10.1016/S0966-9795(99)00029-1

[16] Hu, D., Botten, R. R.: Intermetallics, *10*, 2002, p. 701. doi:10.1016/S0966-9795(02)00047-X

[17] Huang, A., Hu, D., Loretto, M. H., Wu, X.: Intermetallics, *17*, 2009, p. 285. doi:10.1016/j.intermet.2008.09.012

[18] Huang, A., Hu, D., Wu, X., Loretto, M. H.: Intermetallics, *15*, 2007, p. 1147. doi:10.1016/j.intermet.2007.02.002

[19] Hu, D., Huang, A. J., Wu, X.: Intermetallics, *15*, 2007, p. 327. doi:10.1016/j.intermet.2006.07.007

[20] Hu, D.: Intermetallics, *9*, 2001, p. 1037. doi:10.1016/S0966-9795(01)00079-6

[21] Wu, X., Hu, D.: Scr. Mater., *52*, 2005, p. 731. doi:10.1016/j.scriptamat.2004.12.021

[22] Lapin, J., Gabalcová, Z., Bajana, O., Daloz, D.: Kovove Mater., *44*, 2006, p. 297.

[23] Clemens, H., Bartels, A., Bystrzanowski, S., Chladil, H., Leitner, H., Dehm, G., Gerling, R., Schimansky, F. P.: Intermetallics, *14*, 2006, p. 1380. doi:10.1016/j.intermet.2005.11.015

[24] Hu, D., Wu, X., Loretto, M. H.: Intermetallics, *13*, 2005, p. 914. doi:10.1016/j.intermet.2004.12.002

[25] Sankaran, A., Bouzy, E., Humbert, M., Hazotte, A.: Acta Mater., *57*, 2009, p. 1230. doi:10.1016/j.actamat.2008.11.012

[26] Dey, S. R., Bouzy, E., Hazotte, A.: Scr. Mater., *57*, 2007, p. 365. doi:10.1016/j.scriptamat.2007.04.015

[27] Jiang, H., Zhang, K., Hao, X. J., Saage, H., Wain, N., Hu, D., Loretto, M. H., Wu, X.: Intermetallics, *18*, 2010, p. 938. doi:10.1016/j.intermet.2010.01.006

[28] Saage, H., Huang, A. J., Hu, D., Loretto, M. H., Wu, X.: Intermetallics, *17*, 2009, p. 32. doi:10.1016/j.intermet.2008.09.006

[29] Lapin, J., Pelachová, T., Dománková, M.: Intermetallics, *19*, 2011, p. 814. doi:10.1016/j.intermet.2010.11.023

[30] Lapin, J., Pelachová, T., Witusiewicz, V. T. T., Dobročka, E.: Intermetallics, *19*, 2011, p. 121. doi:10.1016/j.intermet.2010.09.016

[31] Lapin, J., Marek, K.: J. Alloys Compd., *735*, 2018, p. 338. doi:10.1016/j.jallcom.2017.11.076

[32] Guyon, J., Hazotte, A., Bouzy, E.: J. Alloys Compd., *656*, 2015, p. 667. doi:10.1016/j.jallcom.2015.09.179

[33] Hu, D., Yang, C., Huang, A., Dixon, M., Hecht, U.: Intermetallics, *22*, 2012, p. 68. doi:10.1016/j.intermet.2011.11.003

[34] Hu, D.: Rare Met., *35*, 2016, p. 1. doi:10.1007/s12598-015-0615-1

[35] Kamyshnykova, K., Lapin, J.: Vacuum, *154*, 2018, p. 218. doi:10.1016/j.vacuum.2018.05.017

[36] Lin, J. P., Zhao, L. L., Li, G. Y., Zhang, L. Q., Song, X. P., Ye, F., Chen, G. L.: Intermetallics, *19*, 2011, p. 131. doi:10.1016/j.intermet.2010.08.029

[37] Hecht, U., Witusiewicz, V., Drevermann, A., Zollinger, J.: Intermetallics, *16*, 2008, p. 969. doi:10.1016/j.intermet.2008.04.019

[38] Li, M., Xiao, S., Xiao, L., Xu, L., Tian, J., Chen, Y.: J. Alloys Compd., *728*, 2017, p. 206. doi:10.1016/j.jallcom.2017.08.211

[39] Schwaighofer, E., Rashkova, B., Clemens, H., Stark, A., Mayer, S.: Intermetallics, *46*, 2014, p. 173. doi:10.1016/j.intermet.2013.11.011

[40] Cheng, T. T.: Intermetallics, *8*, 2000, p. 29. doi:10.1016/S0966-9795(99)00063-1

[41] Kartavykh, A. V., Gorshenkov, M. V., Tcherdyntsev, V. V., Podgorny, D. A.: J. Alloys Compd., *586*, 2014, p. S153. doi:10.1016/j.jallcom.2013.03.104

[42] Veeraraghavan, D., Wang, P., Vasudevan, V. K.: Acta Mater., *51*, 2003, p. 1721. doi:10.1016/S1359-6454(02)00572-4

[43] Dey, S. R., Bouzy, E., Hazotte, A.: Intermetallics, *14*, 2006, p. 444.

[44] Denquin, A., Naka, S.: Acta Mater., *44*, 1996, p. 353. doi:10.1016/1359-6454(95)00168-6

[45] Yang, J., Wang, J. N., Wang, Y., Xia, Q.: Intermetallics, *11*, 2003, p. 971. doi:10.1016/S0966-9795(02)00126-7

[46] Thomas, M., Bacos, M.-P.: Aerosp. Lab, *3*, 2011, p. 1.

[47] Denquin, A., Naka, S.: Acta Mater., *44*, 1996, p. 343. doi:10.1016/1359-6454(95)00167-4

[48] Lapin, J., Klimová, A.: J. Mater. Sci. Lett., *22*, 2003, p. 1275. doi:10.1023/A:1025462220021

[49] Lapin, J., Klimová, A.: Kovove. Mater., *41*, 2003, p. 1.

[50] Zhang, W. J., Evangelista, E., Francesconi, L.: Mater. Sci. Eng. A, *220*, 1996, p. 15. doi:10.1016/S0921-5093(96)10435-4

[51] Kim, Y.-W., Kim, S.-L.: JOM, *70*, 2018, p. 553. doi:10.1007/s11837-018-2747-x

[52] Lapin, J., Kamyshnykova, K.: Intermetallics, *98*, 2018, p. 34. doi:10.1016/j.intermet.2018.04.012